Design and Implementation of a Planar Transformer With Fractional Turns for High Power Density *LLC* Resonant Converters

Yu-Chen Liu, *Senior Member, IEEE*, Chen Chen, *Student Member, IEEE*, Kai-De Chen, *Student Member, IEEE*, Yong-Long Syu, *Student Member, IEEE*, De-Jia Lu, Katherine A. Kim, *Senior Member, IEEE*, and Huang-Jen Chiu, *Senior Member, IEEE*

***Abstract*—This article proposes an isolated *LLC* resonant converter with MHz-level switching frequency that can achieve zero-voltage switching in the full-load range. In the proposed converter, conventional silicon devices are replaced with wide band-gap gallium nitride devices to reduce switching losses in the power device. A planar transformer structure with reduced winding length on the secondary side is proposed, which utilizes flux cancellation and reduces core loss while maintaining a low core volume. The path of the secondary winding is a fraction of a full turn, which reduces secondary-side losses while maintaining a turns ratio of 16:1. This planar transformer achieves the goals of decreasing core loss and volume while increasing power density. Within a limited circuit layout area, optimal points for the efficiency of core loss and copper loss were calculated. The magnetic simulation software ANSYS Maxwell was employed to verify whether the actual circuit behavior of this planar transformer conformed to the design theory. Finally, a resonant converter was achieved with a switching frequency operating at 1 MHz, input voltage of 380 V, output voltage of 12 V, output power of 800 W, power density of 55 W/cm^3, and maximum efficiency of 96.5%.**

***Index Terms*—DC–DC power conversion, resonant power conversion transformer cores, transformer windings, transformers.**

I. Introduction

With the development related to the global race into the Industry 4.0 era, demands for energy are increasing. The technological evolution of the Internet of Things, big data analysis, artificial intelligence, and cloud computing has led researchers to turn their attention to energy conservation. In 2014, according to the reported data, energy consumed by computer, communication, and server power sources is accounted for 1.8% of the United States' total electricity consumption. Furthermore, electricity consumption is increasing annually; the total in the United States is estimated to reach 73 billion kW by 2020 [1]. Therefore, energy waste can be considerably reduced if the conversion efficiency of power supplies can be effectively enhanced. At the same time, various industries are demanding power supplies with smaller volume at the same power rating.

Following the rapid development of equipment for datacenters and cloud servers, numerous types of high-efficiency dc–dc converters have been widely employed, such as the phase-shift full-bridge converter [2]–[5] and *LLC* resonant converter [6]–[8]. The phase-shift full-bridge converter can achieve zero-voltage switching (ZVS) of the primary-side switch [9]–[11] through the energy stored by the leakage inductance of the transformer. However, its ZVS condition is related to the output load, and the switching loss of the power switch cannot be reduced at a light load. When the switching frequency reaches the MHz level, switching loss remains high even with the use of wide band-gap devices. Therefore, for the pursuit of high power density and high conversion efficiency, applying phase-shift full-bridge converters to high-frequency operations at the MHz level is not suitable. By contrast, when the switch operating frequency of an *LLC* series resonant converter is between the first and second resonant frequencies, the ZVS conditions of its power switch are unrelated to load; furthermore, it is characterized by the ZVS of the primary-side switch and the zero-current switching (ZCS) of the secondary-side rectifier switch [12], [13]. This approach can substantially reduce switching loss and electromagnetic interference [14]–[16] of the converter at high frequencies.

To achieve high power density and high efficiency of the converter, the volume of the magnetic component can be decreased through increasing the switching frequency. However, the switching loss of the power switch as well as the core and copper losses of the converter also increases as the frequency increases. The power device and magnetic component must be optimized to solve these difficulties. Although *LLC* resonant

Manuscript received December 21, 2019; revised May 25, 2020 and August 4, 2020; accepted September 22, 2020. Date of publication October 6, 2020; date of current version January 22, 2021. This work was supported in part by the National Science Council of Taiwan under MOST Grants 108-2221-E-197 -016, 108-2218-E-008 -007, and 109- 2218-E-008- 006. Recommended for publication by Associate Editor D. Maksimovic. *(Corresponding author: Yu-Chen Liu.)*

Yu-Chen Liu is with the Department of Electrical Engineering, National I-Lan University, Yilan 26047, Taiwan (e-mail: ycliu@niu.edu.tw).

Chen Chen, Kai-De Chen, and Yong-Long Syu are with the Department of Electronics and Computer Engineering, National Taiwan University of Science and Technology, Taipei 10607, Taiwan (e-mail: d10502204@mail.ntust.edu.tw; a0988138263@gmail.com; x452800@gmail.com).

De-Jia Lu and Huang-Jen Chiu are with the Department of Electronic Engineering, National Taiwan University of Science and Technology, Taipei 10607, Taiwan (e-mail: m10602c06@mail.ntust.edu.tw; hjchiu@mail.ntust.edu.tw).

Katherine A. Kim is with the Department of Electrical Engineering, National Taiwan University, Taipei 10617, Taiwan (e-mail: kakim@ntu.edu.tw).

Color versions of one or more of the figures in this article are available online at https://ieeexplore.ieee.org.

Digital Object Identifier 10.1109/TPEL.2020.3029001

converters possess ZVS to reduce high-frequency switching losses, they nonetheless exhibit exceedingly high turn-OFF losses when using conventional silicon devices. The use of a wide band-gap device gallium nitride (GaN) [17]–[19] to replace conventional silicon devices is an effective method for reducing turn-OFF losses. Because GaN devices have a smaller parasitic capacitor, their switching speed is substantially higher than that of conventional silicon devices, making them more suitable for switching at the MHz level. The ZVS characteristic of *LLC* resonant converters and the use of wide band-gap devices can effectively reduce the switching loss of a power device at MHz switching frequencies. Therefore, the design of the magnetic component is the primary challenge for high-frequency *LLC* resonant converters in terms of efficiency and power density.

The primary transformer losses for *LLC* resonant converters are core loss and copper loss. Core loss of a high-frequency core can be further examined from two perspectives: the material selection and the flux cancellation method. The former can be obtained according to user manuals provided by core material suppliers, such as Ferroxcube, TDK, and ACME. If a core material of 50–200 kHz is used at a switching frequency of 1 MHz, its core loss will increase more than several tens of times. Therefore, according to previous studies [20], [21], core materials that are suitable for use at different frequencies can be obtained. This approach is based on the perspective of core materials, and the further reduction of core losses following the selection of an appropriate core material presents another challenge.

In the literature, several methods for reducing core loss through flux cancellation have been proposed. These methods can be further divided into using numerous vertically stacked cores to enable flux cancellation in the stack [22], and moving the winding position from the center leg on the EI core to the outer leg and having the winding rewound in the opposite direction for flux cancellation to be achieved on the center leg [23], [24]. Although both methods can effectively reduce core losses, the former method entails stacking the core, which decreases the power density of the converter. Thus, the latter method is more suitable for achieving increased power density.

In addition, the transformer copper loss of *LLC* resonant converters can be examined from the perspectives of power density and loss. Conventional transformers are generally wound using litz wires. By comparison, a printed circuit board (PCB) layout has an advantage over a conventional transformer in which it requires a smaller window area than conventional transformer for the winding wire [25], [26]. To achieve high power density, the present study employed a PCB layout to replace conventional litz wire winding for the transformers.

Another method for reducing copper losses involves using circuit architecture and transformer winding. Regarding the application specification of cloud servers, when the secondary-side output is employed for high-current applications, a center-tap rectifier structure is employed instead of a full-bridge rectifier structure. In a center-tap rectifier structure, a parallel secondary-side synchronous rectifier switch is employed to reduce the conduction loss of the transformer's secondary side as well as that of the synchronous rectifier switch. However, this approach cannot reduce the copper loss on the secondary side of the transformer.

Therefore, studies have proposed the concept of matrix transformer circuit architecture [27], [28]. The matrix transformer splits the main transformer into several transformers and employs a circuit architecture in which the primary-side winding is connected in series and the secondary-side winding is connected in parallel. This method can effectively reduce the current in each secondary winding, thus reducing copper loss. Several methods based on the secondary parallel architecture of the matrix transformer circuit exist for reducing the dc resistance of a transformer winding. Because the selection of different effective core cross-sectional area shapes affects the circumference of each turn on the winding, changes in the shape of this area of the transformer [25], [29] can effectively reduce some winding loss.

Another approach is to change the winding method of the transformer, an example being split-flux transformers [30]–[34]. This design changes the restriction of conventional transformer winding, which requires a full turn, as well as takes advantage of the matrix transformer architecture. This also causes the simultaneous conduction of several secondary sides, forming several fractional-turns on the transformer. For the transformer, however, these in fact constitute one full turn. Such an approach can effectively and substantially reduce the copper loss of a transformer. However, in terms of actual transformer design, Faraday's law dictates that when the number of windings is decreased, the effective cross-sectional area of the core must be increased by the same multiple as the number of winding turns decreased to maintain the same peak flux density. Then, the overall core volume increases as the effective cross-sectional area increases. For example, the core volume in a half-flux (or half-turn) transformer [32], [33] increases twofold, and the core volume in a quarter-flux (or quarter-turn) transformer [34] increases fourfold. In this article, several transformer core structures are discussed. In addition to the integration of the flux cancellation method to reduce core loss, a novel planar winding structure with a fractional turn length on the secondary side is proposed to solve the disadvantages of core losses and volume increase that accompanies a split-flux transformer.

An *LLC* resonant converter was employed in this study, and the switching frequency was operated at the resonant frequency as a dc transformer to achieve the highest conversion efficiency [35], [36]. There is no specific requirement for leakage inductance in this design to regulate the output voltage. If a designer needs a specific leakage inductance to operate over a wide input voltage range or adjusting voltage gain to regulate the output voltage, the work in [26] and [29] provide information to address leakage inductance. For the proposed converter, a wide band-gap device GaN was employed to reduce the switching loss of high-frequency application. In the proposed transformer, the primary winding used flux cancellation concepts for the windings to decrease core loss. PCB windings were used to achieve a high-frequency planar transformer, and interleaving was used for the winding arrangement to reduce the magnetomotive force (MMF), thereby decreasing the ac resistance loss [23], [24].

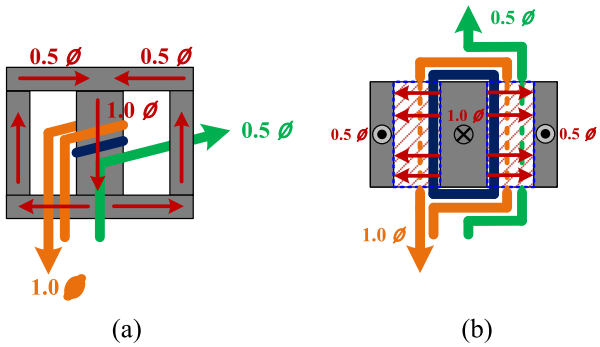

Fig. 1. Induced flux of a half-flux transformer. (a) Side view. (b) Top view.

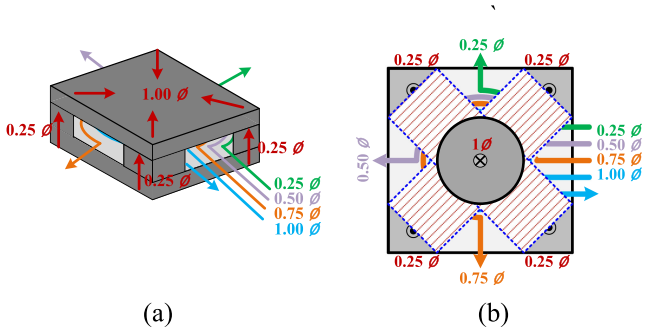

Fig. 2. Induced flux of the quarter-turn transformer. (a) Side view. (b) Top view.

Ultimately, the proposed planar transformer structure can achieve 16 turns on the primary winding with less than a full turn's length on the secondary winding. However, the turns ratio of the transformer exhibits an effect of 16:1. This structure reduces the dc resistance loss of the secondary side and decrease core volume to increase power density. Parametric equations were employed for the design of the transformer dimensions. Using the limited usable area of the circuit board, optimal parameters were found for core loss and copper loss, and the magnetic simulation software ANSYS Maxwell was used to confirm the flux balance of the proposed transformer as well as whether its functions conformed to the design concept of the transformer. The contribution of this article is the design and analysis of a unique transformer structure that combines the advantages of the matrix transformer UI core and the reduced winding length of split-flux transformers to reduce transformer volume while minimizing losses. In the experiment, the final *LLC* resonant converter achieved an operating frequency of 1 MHz, input voltage of 380 V, output voltage of 12 V, output power of 800 W, maximum efficiency of 96.5%, and power density of 55 W/cm^3.

II. Analysis of Flux Induced on the Secondary Side of the Transformer

This section examines differences in the induced flux of the secondary-side winding of a split-flux transformer when different core structures are adopted, which result in differing induced voltages on the secondary side. Previous studies proposed a half-flux transformer with an EI core structure [32], [33], as shown in Fig. 1. Assume that the primary winding is wound counterclockwise on the center leg. The secondary winding may be wound in the form of an equivalent full or half-turn, as shown by the orange line and green line in Fig. 1, respectively. Faraday's Law of electromagnetic induction is shown in (1), where v is the induced voltage, n is the number of turns, and ϕ is the magnetic flux passing through the circuit. The magnitude of the secondary induced voltage is related to the turns ratio of the transformer and the magnetic flux generated on the primary side.

To simplify the following analysis, it is assumed that windings on the primary side of the transformer are all one turn, and the magnetic flux generated on the primary side is 1ϕ. Fig. 1 shows that the magnetic flux generated by the primary winding on the center leg is 1ϕ, where the cross-sectional area of the outer leg of the conventional EI core is one-half of the center leg. According to the theory of magnetic resistance, the magnetic flux flowing into the outer leg is 0.5ϕ. The closed-loop magnetic circuit passes through by the secondary winding of the transformer, and although the green line only passes through a 0.5ϕ closed-loop magnetic circuit, the orange line passes through two 0.5ϕ closed-loop magnetic circuits. The orange line represents a conventional transformer that employs a secondary winding structure with full turns; its induced voltage is the same as the primary-side winding. The green line represents the half-flux transformer structure proposed in [32] and [33]. Because the flux of the closed-loop magnetic circuit through which the secondary winding passes is only 0.5ϕ, the induced voltage is half of the voltage on the primary side

$$v = -n\frac{d\phi}{dt}. \tag{1}$$

Next, the application principle of a quarter-flux transformer proposed in [34] is discussed, which is shown in Fig. 2. When the primary winding is wound counterclockwise around the center leg, the flux generated is 1ϕ. In the core structure, the sum of the cross-sectional areas of the four outer legs is equal to the cross-sectional area of the center leg. According to the theory of magnetic resistance, the flux flowing into each outer leg is 0.25ϕ. In the closed-loop magnetic circuit formed by the secondary winding of the transformer, the green, purple, orange, and blue lines pass through closed-loop magnetic circuits of 0.25ϕ to four times 0.25ϕ, respectively. Therefore, the induced voltages of these four lines are 0.25 times the primary side voltage to one time the primary voltage, respectively.

The proposed design integrates the design methods suggested in [30]–[34] to achieve a split-winding planar transformer. Because the number of turns on the secondary winding were no longer a full turn, the number of primary turns was decreased to maintain the same output voltage as that of the full-turn transformer. For example, with the specifications of a 380-V input and 12-V output, the primary and secondary turns ratio of the transformer is usually 16:1. For a half-flux transformer, however, this ratio becomes 8:0.5, whereas for a quarter-flux transformer it would be 4:0.25. Although the split-flux transformer can reduce copper losses of the primary and secondary sides, at a fixed peak flux density, the effective cross-sectional area of the core must increase proportionally to counteract the increase in peak

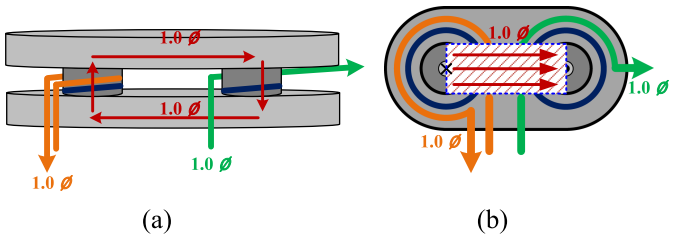

Fig. 3. Schematic of the induced flux of the half-flux transformer. (a) Side view. (b) Top view.

flux density caused by a decrease in the number of primary turns. For example, the core effective cross-sectional areas of the half-flux transformer and quarter-flux transformer must increase by two and four times, respectively, compared with the full-flux transformer to achieve the same peak flux density. This not only increases the core volume, but also decreases the power density of the converter.

To overcome the core volume and loss increases caused by a split-flux transformer, this article proposes a method of applying a core structure that achieves flux cancellation with a UI core with fractional turns on the secondary side to reduce winding length, as shown in Fig. 3. The primary windings are wound clockwise around the left leg and counterclockwise around the right leg, generating a flux of 1ϕ. Therefore, the core structure used at this time only has two legs, which differs from conventional split-flux core; the flux flowing through the two cylinders are both 1ϕ. Therefore, although the orange line and green line pass through one turn and a half-turn, respectively, the induced flux of the secondary side remains 1ϕ. This means that when the transformer employs the winding method of the green line, the induced flux of the secondary winding is 1ϕ as long as the winding passes through the transformer window, even if the winding length is less than a full turn. Thus, even when the input voltage is 380 V and output voltage is 12 V, the turns ratio can be maintained at 16:1. The same peak flux density can be maintained without needing to increase the core's effective cross-sectional area.

In the proposed core structure, the induced magnetic flux on the secondary side is not affected by the winding method or the length of the winding. The induced magnetic flux on the secondary side is only related to the primary magnetic flux and the number of passes through the closed magnetic loop (window of the core). This article has the same induced magnetic flux on the secondary side of the transformer as that of the traditional winding with a full winding. Thus, the secondary-side winding achieves a fractional winding structure at the same maximum magnetic field strength $B_{\max}$ as the traditional transformer, but increased core volume associated with previous split-flux transformer designs can be avoided.

Table I compares the aspects of different high-frequency transformer winding methods. The proposed UI planar transformer with fractional turns to reduce the secondary winding length has approximately half the secondary copper loss compared with a matrix transformer and half the core volume and loss compared with a half-flux transformer. Furthermore,

TABLE I
COMPARISON OF DIFFERENT TRANSFORMER STRUCTURES

Transformer Structure	Matrix [24]	Half-flux [32-33]	Quarter-flux [34]	UI with fractional turns
Frequency	1 MHz	1 MHz	1 MHz	1MHz
Turns ratio	16 : 1	8 : 0.5	4 : 0.25	16 : 1
Primary turns	16	8	4	16
Secondary turns	1	0.5	0.25	0.5 (length)
A_e	A_e	2 A_e	4 A_e	A_e
Volume	Vel	2 Vel	4 Vel	Vel

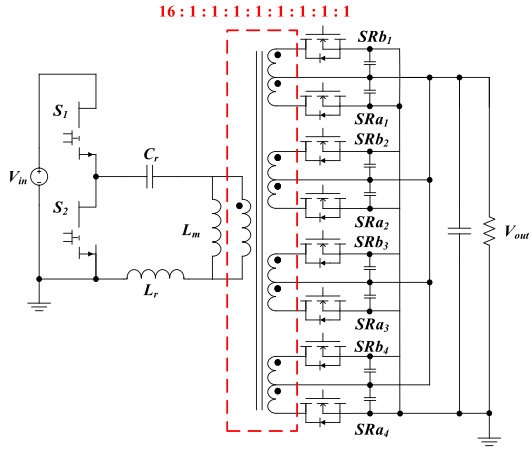

Fig. 4. Circuit diagram of the proposed transformer and *LLC* converter.

compared with a quarter-flux transformer, although the primary and secondary winding losses of the proposed transformer are four and two times, respectively, its core volume and loss are 0.25 times, still giving it a substantial advantage for achieving the goals of high power density and high efficiency.

III. OPERATING INTERVAL OF THE PROPOSED TRANSFORMER

This section discusses the operation of the *LLC* converter with 0.5 turns on the secondary side. Fig. 4 is the circuit diagram, where V_{in} is the input voltage; V_{out} is the output voltage; S_1 and S_2 are the primary power devices using GaN components; L_r and C_r are the resonant inductor and resonant capacitor, respectively; L_m is the magnetizing inductor of the transformer; and SRa and SRb are the positive and negative half-cycle rectifier switches for the secondary side, respectively. The number of turns on the primary side of the transformer is 16, and there are 0.5 turns for each secondary center tap, thus achieving a 380-V input and 12-V output. The primary and secondary windings of the transformer are wound on the two outer legs of the core, with 16 turns for the primary winding, as shown in Fig. 5(a). There are 0.5 turns for the secondary winding, as shown in Fig. 5(b).

During the positive half-cycle, the primary upper switch S_1 is ON and the lower switch S_2 is OFF. As shown in Fig. 6, the current direction of the primary side is counterclockwise for the left leg and clockwise for the right leg, causing an induced

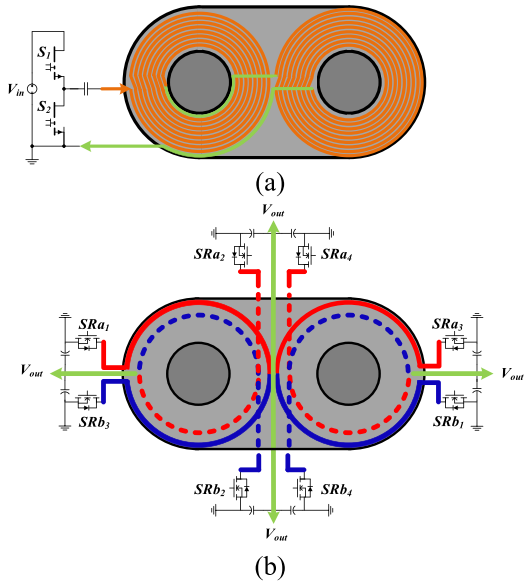

Fig. 5. Schematic of transformer winding. (a) Primary-side winding. (b) Secondary-side winding.

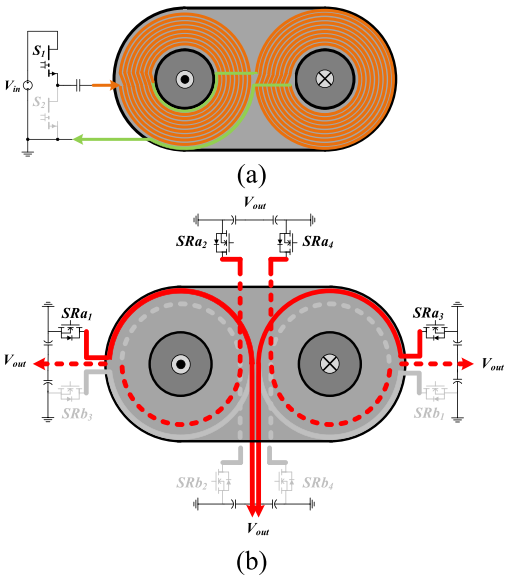

Fig. 7. Current path of the positive half-cycle winding. (a) Primary side. (b) Secondary side.

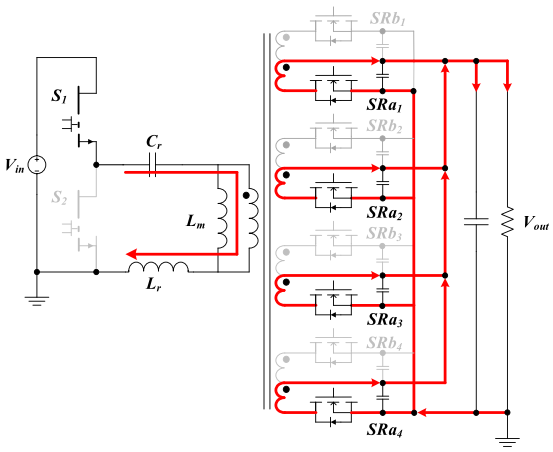

Fig. 6. Current path of the positive half-cycle.

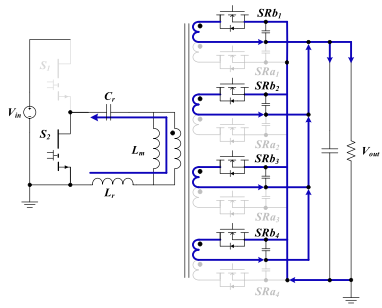

Fig. 8. Current path of the negative half-cycle.

magnetic field inside the core. The direction of the magnetic field is depicted in Fig. 7(a). According to Faraday's law, the secondary side of the transformer generates a clockwise current in the left leg, whereas a counterclockwise current is generated in the right leg against the applied magnetic field. The secondary side current of the transformer flows from the ground (GND) to SRa_1, SRa_2, SRa_3, and SRa_4, then flows through the secondary winding, and finally flows out toward the V_{out} point. As shown in Fig. 7(b), any point V_{out} is connected to the same point as the remaining three points, and any point GND is connected to the same point as the remaining GND points. Therefore, the secondary winding can be viewed as a parallel relationship, and the equivalent number of secondary turns is 0.5. Four sets of secondary side joints are separately wound around the left and right legs of the core, and the secondary winding of each leg passes through the core window, seeing the full flux of the core. The generated magnetic field is similar to that of a conventional center leg wound for a full turn. Thus, the magnetic field in the transformer does not develop an imbalance.

During the negative half-cycle, the primary upper switch S_1 is OFF and the lower switch S_2 is ON. As shown in Fig. 8, the primary current direction comprises a clockwise direction for the left leg and counterclockwise direction for the right leg, which generate an induced magnetic field inside the core. The magnetic field direction is shown in Fig. 9(a). According to Faraday's law, the secondary side of the transformer generates a current in the counterclockwise direction on the left leg, and a clockwise current on the right leg against the applied magnetic field. The secondary current of the transformer flows from GND to SRb_1, SRb_2, SRb_3, and SRb_4, then flows through the secondary winding, and finally flows out toward point V_{out}. Any point V_{out} is connected to the same point as the remaining three points, and any point GND is connected to the same point as the remaining GND points, as shown in Fig. 9(b). When any switch is turned ON and current flows in the transformer, the secondary winding of the transformer sees the full flux induced through the core. Therefore, this method is equivalent to conventional transformer winding in terms of magnetic flux

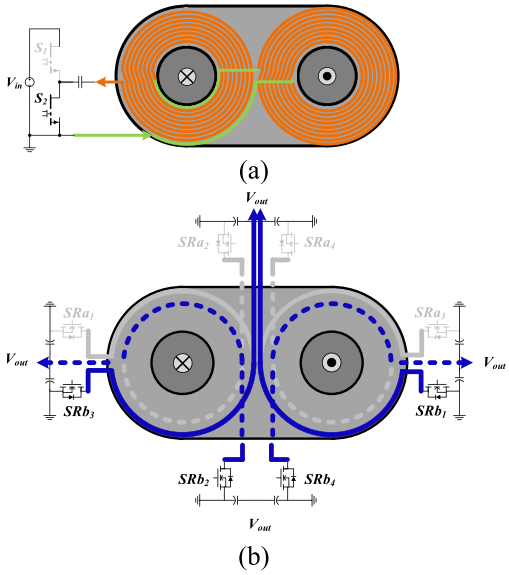

Fig. 9. Current path of the negative half-cycle winding. (a) Primary side. (b) Secondary side.

and does not possess the disadvantages of core volume and loss increases that other split-flux transformers do. Compared with transformers with conventional winding methods, this method effectively reduces copper losses on the secondary winding of the transformer under large output currents.

IV. Structural Analysis and Design of the Planar Transformer Core

This section introduces the core structure and design of the proposed planar transformer. Using a parametric design under a limited area for circuit layout, the optimal design parameters to reduce core loss were determined. A placement with minimal ac resistance loss was found, which is particularly challenging to minimize at high switching frequencies in the MHz range. ANSYS Maxwell was employed to analyze the secondary-side winding length of the proposed transformer, as well as to ensure that positive and negative half-cycle imbalance would not occur in each center-tap current of the secondary side.

To achieve the highest efficiency of the *LLC* resonant converter, the operating frequency was fixed at the resonant frequency and the *LLC* resonant converter was used as a dc transformer. The circuit specifications in this article were as follows: an input voltage of 380 V, output voltage of 12 V, and output wattage of 800 W. The core structure was parameterized to examine the relationship between core loss and copper loss and to select the appropriate core dimensions, as shown in Fig. 10, where r is the effective cross-sectional area radius of the core, R is the maximum length of the winding radius, T is the thickness of sheet I, and Z is the cylinder height.

In consideration of the loss characteristics of high-frequency materials, the peak flux density should not exceed 100 mT. The usage manual of magnetic materials reveals that when the peak flux density of a ferrite core exceeds 100 mT, core loss increases sharply. Therefore, this article selected a unit volume

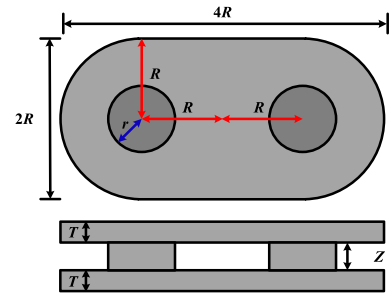

Fig. 10. Graph of core dimensions.

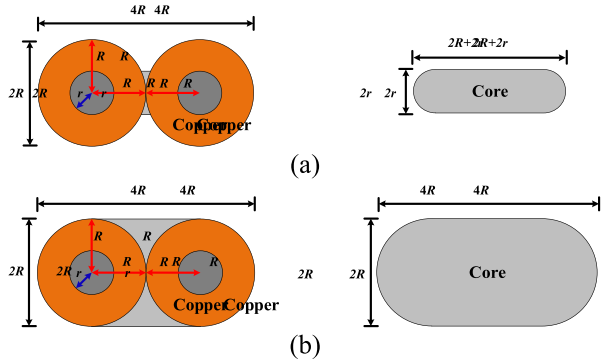

Fig. 11. Diagram of core dimensions. (a) Original core. (b) Optimized core.

loss of 600 kW/m^3 to execute the following design. Hitachi's high-frequency magnetic material ML91S was used as the ferrite core material. When the core loss per unit volume was 600 kW/m^3 and the switching frequency was 1 MHz, the peak flux density was found to be 74 mT. Equation (2) was used to obtain the effective cross-sectional area of the core at this time, A_e, at 39.79 mm^2, and the radius r at 3.56 mm. In the following equation, V_{in} is the input voltage of the circuit, at 380 V; B_m is the peak flux density with a value of 74 mT; N_p is the number of turns in the primary winding, 16 turns; and f_{sw} is the operating frequency of the circuit, at 1 MHz

$$A_e = \pi \cdot r^2 = \frac{V_{\text{in}}}{8 \cdot B_{\max} \cdot N_p \cdot f_{\text{sw}}}. \tag{2}$$

Next, using the parametric equation α of the core, as shown in (3); the larger the value of α, the larger the core winding radius R. The value of the winding radius R subtracting the core effective cross-sectional area radius r is the winding width of the core. A greater width results in smaller dc resistance of the transformer winding as well as smaller copper loss

$$R(\alpha) = \alpha \cdot r. \tag{3}$$

Because the flux density must be consistent in each path to avoid complications with magnetic field lines and hotspot concentration, the core leg effective cross-sectional area must be equal to the cross-sectional area of the magnetic flux flowing through sheet I. The conventional UI core structure is shown in Fig. 11(a), and the thickness of sheet I at this time is calculated by (4). To reduce the overall height of the transformer, the top

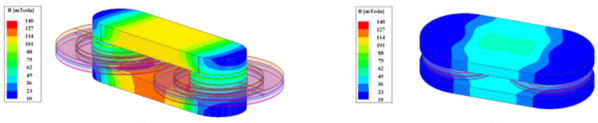

(a) (b)

Fig. 12. Maxwell simulation diagram. (a) Original core. (b) Optimized core.

and bottom covers of the transformer were optimized. Fig. 11(a) illustrates that when the core structure of the transformer is the same as that of the conventional UI core, the area occupied by the circuit layout of the transformer and the area of the transformer winding to obtain the occupancy area of the entire transformer must be considered. The total area of the transformer at this time was $8R^2$. Therefore, using the same total area, this article proposed increasing the magnetic circuit of the transformer outward while maintaining the same effective cross-sectional area. Simultaneously, the thicknesses of the top and bottom covers of the transformer were decreased. The core shape after the volume increase is shown in Fig. 11(b). The thickness of sheet I can be rewritten as (5); because α is the ratio of the winding radius and core radius, and because the winding radius must be greater than the core radius, α must be greater than 1. Additionally, this means that the thickness of the I sheet in Fig. 11(b) is smaller than that in Fig. 11(a). The total volume of the core can be expressed using (6)

$$T = \frac{\pi r}{2} \tag{4}$$

$$T(\alpha) = \frac{\pi r}{2\alpha} \tag{5}$$

$$\mathrm{Vel}(\alpha) = 2A_e \cdot z + 2\left[4R(\alpha)^2 \cdot T + \pi R(\alpha)^2 \cdot T\right]. \tag{6}$$

Using the Modified Steinmetz equation, core loss can be expressed using parameters as shown in (7), where P_v is the core loss per unit volume, and its value forms an exponential ratio with the values of the operating frequency and peak flux, as shown in (8). Among these, C_m, x, and y can be obtained from the core materials manual of the manufacturer. Finally, different volume sizes can be obtained according to differences in the core proportional parameter α, thereby obtaining core loss. As the α value and core volume increase, assuming a fixed P_v, core loss also increases accordingly

$$\mathrm{Coreloss}(\alpha) = P_v \cdot \mathrm{Vel}(\alpha) \tag{7}$$

$$P_v = \left(C_m \cdot f_{\mathrm{eq}}^{x-1} \cdot B_{\max}^{y}\right) \cdot f_{\mathrm{sw}}. \tag{8}$$

Next, ANSYS Maxwell was employed to verify differences between before and after the thickness optimization of the core I sheet. Fig. 12 shows that although the peak flux density in this article was designed to be 74 mT, magnetic flux was not evenly distributed on the magnetic circuit of the core. Therefore, using Maxwell, this work observed that the highest flux density at this time was approximately 114 mT. In Fig. 12(b), additional volume of the core is added with a peak flux density of approximately 74 mT, which is exceedingly close to the original design value. Using the magnetic material core loss parameter, it was found that when the core peak flux density exceeded 100 mT, core loss increased sharply. In Fig. 12(a), when α was 2.45, the core loss was 9 W, and in Fig. 12(b) after the thickness optimization of sheet I it was 3.7 W. This optimization method decreases the core height under condition of the same occupancy area as well as effectively mitigates the increase in core loss caused by the uneven distribution of peak flux density.

Next, this section examines copper loss. First, the dc resistance of the transformer winding can be expressed using the following equation, where the winding length is represented by "Length," ρ is the resistivity of the copper wire, h is the winding thickness, and "Width" is the width of the copper wire:

$$R_{\mathrm{copper}}(\alpha) = \rho \frac{\mathrm{Length}(\alpha)}{h \cdot \mathrm{Width}(\alpha)}. \tag{9}$$

Considerations of the thickness of the winding wire require observations of the effect of ac resistance. Based on the assumptions of Dowell's equation [37], under the condition of a sinusoidal current at the excitation source for copper foil, the influence of the skin effect on ac resistance can be expressed using (10). The influence of the proximity effect on ac resistance is expressed using (11). For the application of multilayer winding, the influence of the proximity effect substantially exceeds that of the skin effect, and its influence can be expressed by the size of m, where m represents the MMF corresponding to each layer. The minimum MMF can be achieved when a full interleaving winding method is used; thus, the influence of m can be minimized. However, if a non-full-interleaving winding method is used, the ac resistance corresponding to windings with larger MMF increases substantially. The total ac resistance is obtained by summing (10) and (11), as shown in (12)

$$R_{\mathrm{ac\_skin}} = \frac{\xi}{2} \cdot \frac{\sinh(\xi) + \sin(\xi)}{\cosh(\xi) - \cos(\xi)} \cdot R_{\mathrm{dc}} \tag{10}$$

$$R_{\mathrm{ac\_proximity}} = \frac{\xi}{2} \cdot (2m-1)^2 \cdot \frac{\sinh(\xi) - \sin(\xi)}{\cosh(\xi) + \cos(\xi)} \cdot R_{\mathrm{dc}} \tag{11}$$

$$R_{\mathrm{ac\_total}} = R_{\mathrm{ac\_skin}} + R_{\mathrm{ac\_proximity}}. \tag{12}$$

Finally, based on the previous calculations of core loss and ac copper loss, the total transformer loss can be obtained by summing these values, as shown in Fig. 13. The figure reveals that a minimum loss point appears when α is 2.45; this α value was ultimately employed as the final design parameter. A design diagram with core dimensions is shown in Fig. 14, where (a) is the top view of the core and (b) is the side view of the core.

ANSYS Maxwell was used to analyze and verify this concept and whether it could be applied to the winding structure of the transformer, as well as to verify whether the turns ratio of the secondary side conformed to the analysis in the previous section. To obtain accurate simulation results, a 1:1 3-D model of the core was constructed. The method employed in ANSYS Maxwell used the external circuit function, where a capacitor and inductor were connected in series as the resonant tank to the primary side of the transformer, and waveforms were used to generate square wave voltage, crossing the two ends of the capacitor and the

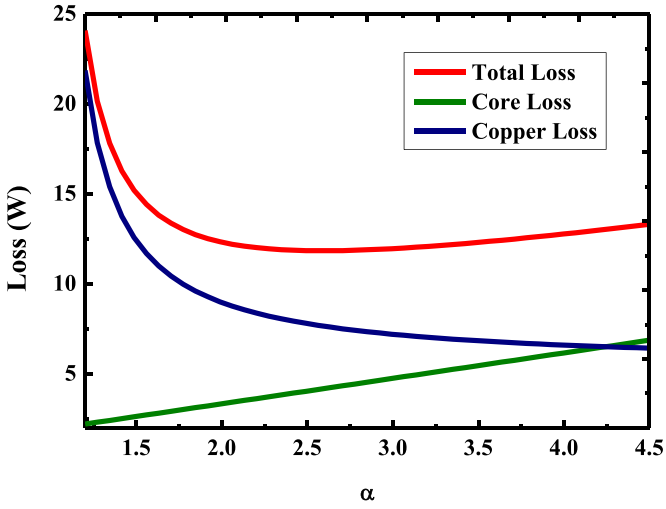

Fig. 13. Relationship between α value and total loss.

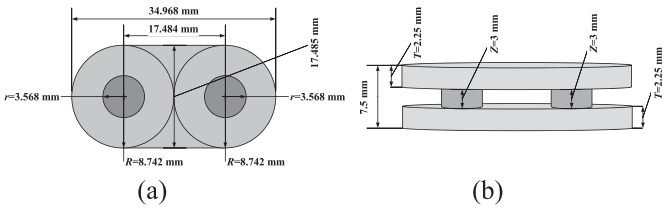

Fig. 14. Actual core size. (a) Core top view. (b) Core side view.

TABLE II
MAXWELL SIMULATION PARAMETERS

Specification Items	Circuit Parameters
Transformer material	ML91S
Resonant capacitor	32 nF
Resonant inductor	768 nH
Transformer voltage source	±190 V
Magnetizing inductor	25 uH
Resonant frequency	1 MHz

inductor and transformer, thereby simulating the exact working condition of the *LLC* resonant converter. Table II presents the simulation parameters. For the proposed transformer, Figs. 15 and 16 reveal that even when the actual winding length of the secondary side is approximately half a turn, the primary-to-secondary voltage ratio of the transformer remains 16:1. Fig. 17 verifies that regardless of when the transformer is conducting in the positive half-cycle or negative half-cycle, the core achieves balanced magnetic flux.

V. EXPERIMENTAL VERIFICATION

This section details the experimental verification of an *LLC* resonant converter with the proposed UI planar transformer with input voltage of 380 V, output voltage of 12 V, output power density of 800 W, and operating frequency of 1 MHz. Components

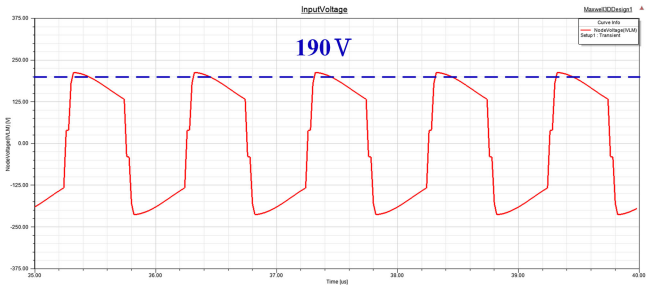

Fig. 15. Transformer's primary voltage stress.

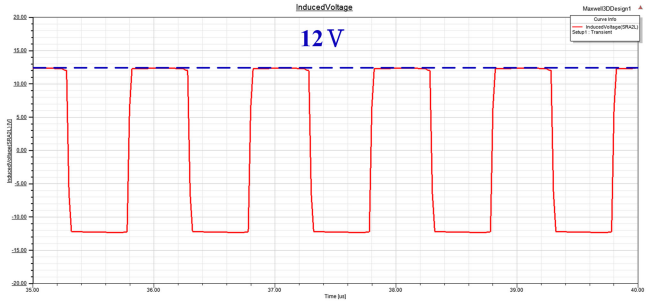

Fig. 16. Transformer's secondary voltage stress.

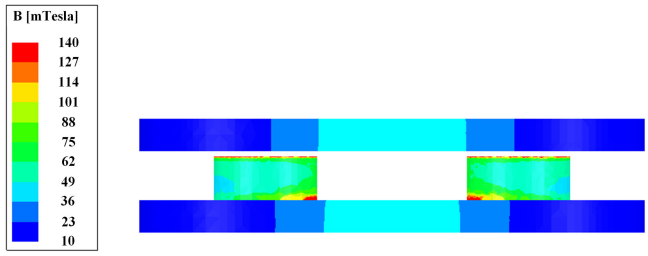

Fig. 17. Balanced flux distribution.

TABLE III
MEASURED *LLC* CONVERTER CIRCUIT SPECIFICATIONS

Specification items	Specification data
Input voltage V_{in}	380 V
Output voltage V_{out}	12 V
Output maximum power P_o	800 W
Resonant frequency f_r	1.015 MHz
Circuit operating frequency f_{sw}	1 MHz

in the 3-D model and the dimensions of the transformer are presented in Fig. 18(a) and (b), respectively. Fig. 18(c) shows the actual core. Fig. 18(d) and (e) shows the circuit layout and current directions, respectively, of the secondary side. The height of the overall circuit was 0.7 cm and the power density of the *LLC* converter was 55 W/cm^3.

Table III presents the circuit specifications in this study. The circuit parameters for the *LLC* resonant converter, switching components, and magnetic materials are shown in Table IV.

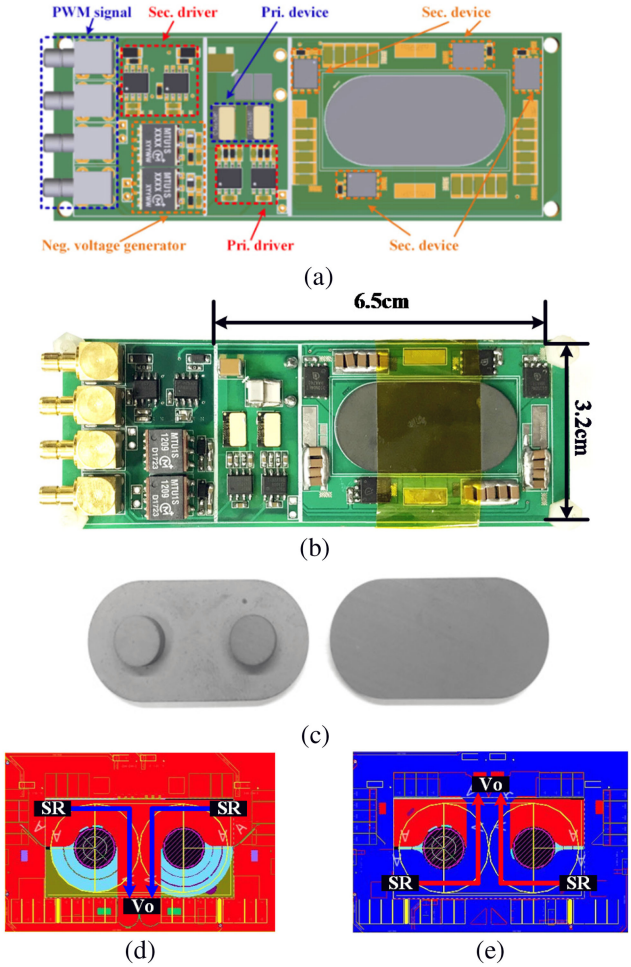

Fig. 18. 3-D model. (a) Component labels. (b) Actual circuit. (c) Actual core. (d) Current directions of the secondary side during the positive half-cycle. (e) Current directions of the secondary side during the negative half-cycle.

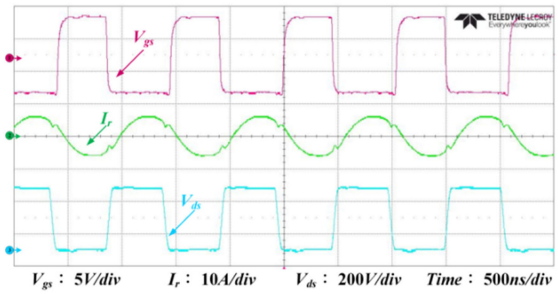

Fig. 19. Primary-side $V_{\rm gs}$, $V_{\rm ds}$, and resonant current.

The measured waveforms of the circuit are shown in Fig. 19, where the output load is 100%, with $I_o = 66.7$ A. The measured waveforms were the resonant tank current of the primary side and the waveform of the primary lower bridge $V_{\rm ds}$.

The measured efficiency curve of the circuit is shown in Fig. 20, where the highest efficiency is 96.5% when the output power is 400 W. The loss analysis of the full load is shown in Fig. 21. According to the loss analysis, the total transformer loss was approximately 13 W, which included core loss and dc and ac copper losses. The switching loss on the primary side was approximately 12 W, which included the turn-OFF switching loss and conduction loss. Because the secondary power switch possessed the characteristics of ZCS, switch loss comprised only the conduction loss, for a total of 13.6 W. Other losses

TABLE IV
CIRCUIT USAGE-RELATED PARAMETERS

Specification	Component/Parameter
Transformer turns ratio	16:1, 0.5 turn length on secondary side
Core material	ML91S
Primary power switch	GS66508T
Secondary synchronous rectifier component	BSC0500NSI
Primary isolated driver IC	SI8271LS
Secondary isolated driver IC	FAN3122
Resonant capacitor	32 nF
Resonant inductor	768 nH
Magnetizing inductor	21 μH

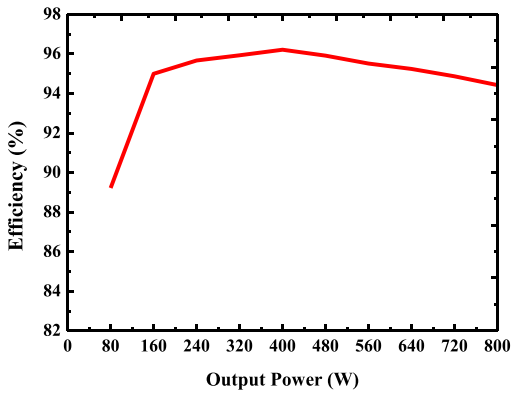

Fig. 20. Experimental efficiency curve of the circuit.

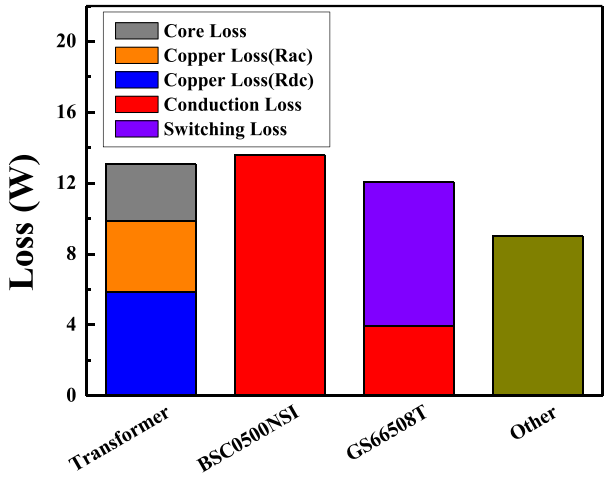

Fig. 21. Loss analysis of the full load.

TABLE V
COMPARISON OF SIMILAR MATRIX TRANSFORMER ATTRIBUTES

	[23]	[24]	[30]	[32]	[34]	This work
Vin/Vo	390V/ 12V	380V/ 12V	120V-380V/5V-20V	380V/ 12V	380V/ 12V	380V/ 12V
Output power	1 kW	800 W	36 W	600 W	1 kW	800 W
Operating frequency	1 MHz	1 MHz	0.5 MHz-1.3MHz	750 kHz	1 MHz	1 MHz
Transformer structure	Matrix		Split-Flux			UI with fractional turns
Turns of primary winding	16	16	8	8	4	16
Turns of secondary winding	1	1	0.5	0.5	0.25	0.5 (length)
Core shape	UI	4 leg	EI	EI	5 leg	UI
Power density	51 W/cm^3	54 W/cm^3	Not mentioned	21.3 W/cm^3	38 W/cm^3	55 W/cm^3
Peak efficiency	95.4 %	97.6 %	91 %	98 %	97 %	96.5 %

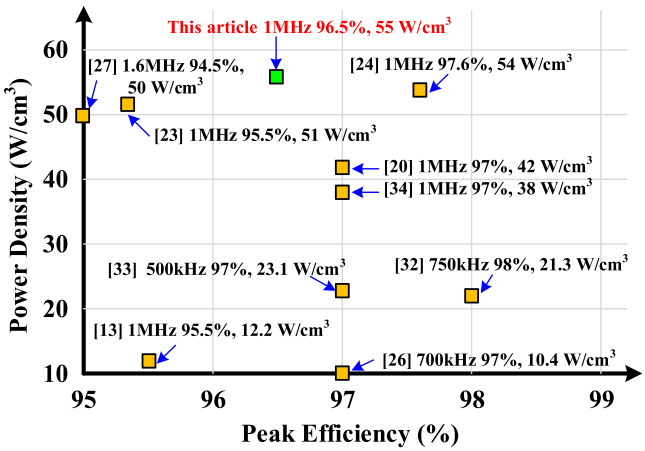

Fig. 22. Power density comparison table.

include circuit winding loss, terminal loss, and input and output capacitor losses.

Fig. 22 presents a power density comparison of various 380 V to 12 V dc–dc converters, where Mu and Lee [20], Huang *et al.* [23], and Fei *et al.* [24] use matrix transformers and operate at 1-MHz switching frequency with transformers that employ flux cancellation to reduce core losses. The proposed planar UI transformer's structure has lower copper loss than the traditional UI matrix transformer. By utilizing the induction of the transformer flux, the proposed transformer also has flux cancellation, such that it achieves lower core loss and copper loss than the traditional UI matrix transformer.

In the *LLC* converter matrix transformer developed in [24], several transformers were integrated together to achieve an overall power density of 54 W/cm^3. The *LLC* converter with the proposed converter achieves a power density that is 1 W/cm^3 higher than [24], but the overall conversion efficiency of this work is 1% lower. Compared to the work in [24], the proposed transformer does not achieve full flux cancellation to reduce the eddy current loss in winding, but the major advantage is the fractional turn winding on the secondary side that reduces the length of the winding and associated losses. Although the results have not shown an advantage in overall converter efficiency, but based on the core structure alone, losses in the transformer for the proposed structure are lower than that of the matrix transformer structure in [24]. A detailed comparison of the different types of losses in each structure is provided in the Appendix.

In [30]–[34], split-flux transformer architecture was presented in which fractional turns were used to reduce secondary copper loss. The transformer structures adopted by Ranjram *et al.* [30] and Li *et al.* [32] are traditional half-flux transformers. Both use an EI core and the secondary winding forms an equivalent half-turn. For the secondary winding method of the transformer in [30] and [32], the difference between the two is only in the rectification structure of the secondary side. In [32], the half-flux transformer structure used has an input voltage of 380 V and an output voltage of 12 V. Therefore, a center-tap structure is adopted at the rectifier side, and the fractional-turn structure effectively reduces copper loss. The quarter-turn transformer in [34] uses a single core with multiple sets of center taps in parallel, and the secondary winding of the transformer uses fractional turns to further reduce copper loss. To reduce the number of primary side primary-side turns to a quarter of the original and maintain the same $B_{\max}$, the cross-sectional area A_e would need to increase four times, such that the overall volume would also increase four times.

For the goal of high power density, the increased core volume associate with previous split-flux transformer designs is a challenge that the proposed design overcomes. Note that the proposed planar transformer design is appropriate for higher input voltage and high step-down ratio applications, like 380-V input to 12-V output, but loses some of its advantages for lower voltage, higher current converter applications. In the present study, the concepts of flux cancellation and fractional turns were combined and flux induction was used to achieve a turns ratio of 16:1, even though the secondary winding length is less than a full turn. The disadvantage of the need for an exponential increase in core volume for a split-flux transformer was solved,

ultimately reaching a power density of 55 W/cm^3. The proposed transformer structure could also be applied to other high step-down converters with multiple windings on one side to achieve high power density.

A comparison of this article and similar transformer structures is shown in Table V. The work in [23] and [24] adopts only the traditional matrix transformer structure, whereas the work in [30], [32], and [34] uses a split-flux transformer structure. In [23] and [24], the secondary winding structure is a full winding; in [30], [32], and this article, the secondary winding length is equivalent to a half-turn; in [34], the secondary winding is equivalent to a quarter-turn. It follows that the copper loss on the secondary side, in [32], [34], and this article, are lower than that in [23] and [24]. For a more detailed comparative analysis of the various split-flux transformers and the proposed structure, see the Appendix.

VI. Conclusion

In this article, a planar transformer with fractional turns on the secondary side was proposed for a high power density *LLC* resonant converter. Using the resonant characteristics of this converter and GaN switches, conduction and turn-OFF losses at a switching frequency of 1 MHz were greatly reduced. For the planar transformer design, flux cancellation was employed to target core losses by placing the primary winding on the outer leg and utilizing reverse windings to reduce core losses. The secondary side of the transformer employed equivalent half-turn winding length to reduce the dc resistance loss while maintaining a 16:1 turns ratio. As a result, power density could be increased and core volume decreased at the same peak flux density. Furthermore, using the core parameter α, an optimized core size was designed with considerations of core loss, copper loss, and power density within a limited circuit layout area. ANSYS Maxwell was employed to verify that the structure of the secondary windings conformed to the theoretical analysis. Finally, the proposed planar transformer for an *LLC* resonant converter was achieved with an output power of 800 W, switching frequency of 1 MHz, maximum efficiency of 96.5%, and power density of 55 W/cm^3.

Appendix

This appendix compares the design differences between the traditional matrix transformer structure, different split-flux transformer structures, and this work. The input voltage is 380 V, the output voltage is 12 V, the output power is 800 W, the switching frequency is 1 MHz, the primary-side topology is a half-bridge structure, and the secondary side consists of four sets of center taps connected in parallel. That is, 16 primary turns, and 1 secondary turn for the traditional transformer; 8 primary turns and 0.5 secondary turns for the half-flux transformer; and 4 primary turns and 0.25 secondary turns for the quarter-flux transformer. The number of primary turns of the transformer proposed in this article is 16 turns, and the length of the secondary-side winding is equivalent to 0.5 turns.

Next, the maximum magnetic field strength $B_{\max}$ from Faraday's Law (13) is set to 76 mT and PUI22 is selected as the single-loop transformer core. Because the primary winding of the half-flux transformer is 8 turns, according to Faraday's Law, the cross-sectional area A_e should be doubled. Therefore, if the core PEI-22 is used, the volume of the quarter-turn transformer would increase fourfold, which is equivalent to four PUI-22. Next, the core loss is calculated. Since $B_{\max}$ of the transformer is the same, the core loss is proportional to the volume according to the modified Steinmetz equation (14). The results, summarized in Table VI, show that the volume and core loss of a quarter-turn transformer is four times that of a full-turn matrix transformer

$$B_{\max} = \frac{V_{\text{in}}}{8 \cdot N_p \cdot f_{\text{sw}} \cdot A_e} \tag{13}$$

$$P_v = \left(C_m \cdot f_{\text{eq}}^{x-1} \cdot B_{\max}^{y}\right) \cdot f_{\text{sw}}. \tag{14}$$

Then, the copper loss of the transformer is calculated. The rms value of the primary current is 2.5 A and of the secondary current is 16.5 A. The winding width of the PUI-22 core is

TABLE VI
Comparison of Similar Transformer Attributes

Transformer structure	Full-Turn Matrix	Half-flux	Quarter-flux	This work
Vin/Vo	380V/ 12V			
Output power	800W			
Operating frequency	1 MHz			
Primary side topology	Half bridge topology			
Secondary side topology	4 Center-tap topology			
Transformer voltage ratio	16:1			
Primary side turns	16	8	4	16
B_{max}	76 mT			
Core size	PUI-22	PEI-22	PUI-22*4	PUI-22
A_e (mm^2)	39.25	78.5	157	39.25
Vol. (mm^3)	1020	2040	4080	1020
Material	ML91S			
Core loss (W)	0.612	1.224	2.448	0.612
Primary side RMS current	2.5 A			
Secondary side RMS current	16.5 A			
Winding width	4 mm			
Copper thickness	2 oz			
Primary copper loss (W)	0.212	0.106	0.053	0.212
Secondary copper loss (W)	4.628	2.314	1.157	2.314
Total loss (W)	5.452	3.644	3.552	3.138

4 mm. The calculation is for a circle, where the thickness of each winding is that of 2-oz copper in a PCB layer. Since the effective current values are the same, the copper loss of the transformer winding is only related to the length of the winding. The winding arrangement and ac resistance R_{ac} calculation are not considered here because it is highly dependent on the exact winding arrangement that depends on the specific application. The loss of the winding can be obtained, as shown in Table VI.

The transformer structure proposed in this article has the same primary winding method as the matrix transformer but the secondary winding method is equivalent to the half-flux transformer. Therefore, primary copper losses are the same as the matrix transformer, whereas the secondary copper losses are the same as the half-flux transformer. Summing the transformer core loss and copper loss in Table VI, the proposed transformer has the best performance in terms of core volume and transformer loss.

REFERENCES

[1] E. Orlando, "United States data center energy usage report," Lawrence Berkeley Nat. Lab., Berkeley, CA, USA, LBNL-1005775, Jun. 2016.

[2] K. Shi, D. Zhang, Z. Zhou, M. Zhang, and Y. Gu, "A novel phase-shift dual full-bridge converter with full soft-switching range and wide conversion range," *IEEE Trans. Power Electron.*, vol. 31, no. 11, pp. 7747–7760, Nov. 2016.

[3] J. Kim, D. Kim, C. Kim, and G. Moon, "A simple switching control technique for improving light load efficiency in a phase-shifted full-bridge converter with a server power system," *IEEE Trans. Power Electron.*, vol. 29, no. 4, pp. 1562–1566, Apr. 2014.

[4] Y. Liu *et al.*, "Integrated magnetics design for a full-bridge phase-shifted converter," in *Proc. IEEE Appl. Power Electron. Conf. Expo.*, 2018, pp. 2110–2116.

[5] B. Chen and Y. Lai, "Switching control technique of phase-shift-controlled full-bridge converter to improve efficiency under light-load and standby conditions without additional auxiliary components," *IEEE Trans. Power Electron.*, vol. 25, no. 4, pp. 1001–1012, Apr. 2010.

[6] H. Wu, T. Mu, X. Gao, and Y. Xing, "A secondary-side phase-shift-controlled LLC resonant converter with reduced conduction loss at normal operation for hold-up time compensation application," *IEEE Trans. Power Electron.*, vol. 30, no. 10, pp. 5352–5357, Oct. 2015.

[7] J. Lee, J. Kim, J. Kim, J. Baek, and G. Moon, "A high-efficiency PFM half-bridge converter utilizing a half-bridge LLC converter under light load conditions," *IEEE Trans. Power Electron.*, vol. 30, no. 9, pp. 4931–4942, Sep. 2015.

[8] F. C. Lee, Q. Li, Z. Liu, Y. Yang, C. Fei, and M. Mu, "Application of GaN devices for 1 kW server power supply with integrated magnetics," *CPSS Trans. Power Electron. Appl.*, vol. 1, no. 1, pp. 3–12, Dec. 2016.

[9] R. Redl, N. O. Sokal, and L. Balogh, "A novel soft-switching full-bridge DC/DC converter: Analysis, design considerations, and experimental results at 1.5 kW, 100 kHz," *IEEE Trans. Power Electron.*, vol. 6, no. 3, pp. 408–418, Jul. 1991.

[10] H. Bai, Z. Nie, and C. C. Mi, "Experimental comparison of traditional phase-shift, dual-phase-shift, and model-based control of isolated bidirectional DC–DC converters," *IEEE Trans. Power Electron.*, vol. 25, no. 6, pp. 1444–1449, Jun. 2010.

[11] G.-B. Koo, G.-W. Moon, and M.-J. Youn, "New zero-voltage-switching phase-shift full-bridge converter with low conduction losses," *IEEE Trans. Ind. Electron.*, vol. 52, no. 1, pp. 228–235, Feb. 2005.

[12] B. Yang, F. C. Lee, A. J. Zhang, and G. Huang, "LLC resonant converter for front end DC/DC conversion," in *Proc. APEC. 17th Annu. IEEE Appl. Power Electron. Conf. Expo.*, 2002, vol. 2, pp. 1108–1112.

[13] D. Fu, F. C. Lee, and S. Wang, "Investigation on transformer design of high frequency high efficiency dc-dc converters," in *Proc. 25th Annu. IEEE Appl. Power Electron. Conf. Expo.*, 2010, pp. 940–947.

[14] Y. Yang, D. Huang, F. C. Lee, and Q. Li, "Analysis and reduction of common mode EMI noise for resonant converters," in *Proc. IEEE Appl. Power Electron. Conf. Expo.*, 2014, pp. 566–571.

[15] D. Fu, P. Kong, S. Wang, F. C. Lee, and M. Xu, "Analysis and suppression of conducted EMI emissions for front-end LLC resonant DC/DC converters," in *Proc. IEEE Power Electron. Specialists Conf.*, 2008, pp. 1144–1150.

[16] B. Li, Q. Li, F. C. Lee, and Y. Yang, "A symmetrical resonant converter and PCB transformer structure for common mode noise reduction," in *Proc. IEEE Energy Convers. Congr. Expo.*, 2017, pp. 5362–5368.

[17] X. Huang, Z. Liu, Q. Li, and F. C. Lee, "Evaluation and application of 600 V GaN HEMT in cascode structure," *IEEE Trans. Power Electron.*, vol. 29, no. 5, pp. 2453–2461, May 2014.

[18] U. K. Mishra, P. Parikh, and Y.-F. Wu, "AlGaN/GaN HEMTs—An overview of device operation and applications," *Proc. IEEE*, vol. 90, no. 6, pp. 1022–1031, Jun. 2002.

[19] J. Millán, P. Godignon, X. Perpiñà, A. Pérez-Tomás, and J. Rebollo, "A survey of wide bandgap power semiconductor devices," *IEEE Trans. Power Electron.*, vol. 29, no. 5, pp. 2155–2163, May 2014.

[20] M. Mu and F. C. Lee, "Design and optimization of a 380–12 V high-frequency, high-current LLC converter with GaN devices and planar matrix transformers," *IEEE J. Emerg. Sel. Topics Power Electron.*, vol. 4, no. 3, pp. 854–862, Sep. 2016.

[21] B. Li, Q. Li, and F. C. Lee, "A WBG based three phase 12.5 kW 500 kHz CLLC resonant converter with integrated PCB winding transformer," in *Proc. IEEE Appl. Power Electron. Conf. Expo.*, 2018, pp. 469–475.

[22] R. Chen, P. Brohlin, and D. Dapkus, "Design and magnetics optimization of LLC resonant converter with GaN," in *Proc. IEEE Appl. Power Electron. Conf. Expo.*, 2017, pp. 94–98.

[23] D. Huang, S. Ji, and F. C. Lee, "LLC resonant converter with matrix transformer," *IEEE Trans. Power Electron.*, vol. 29, no. 8, pp. 4339–4347, Aug. 2014.

[24] C. Fei, F. C. Lee, and Q. Li, "High-efficiency high-power-density LLC converter with an integrated planar matrix transformer for high-output current applications," *IEEE Trans. Ind. Electron.*, vol. 64, no. 11, pp. 9072–9082, Nov. 2017.

[25] Y. C. Liu, C Chen, K. D. Chen, Y. L. Syu, and M. C. Tsai, "High-frequency LLC resonant converter with GaN devices and integrated magnetics," *Energies*, vol. 12, 2019, Art. no. 1781.

[26] Y. Liu, C. Chen, K. Chen, Y. Syu, and N. A. Dung, "High-frequency and high-efficiency isolated two-stage bidirectional DC-DC converter for residential energy storage systems," *IEEE J. Emerg. Sel. Topics Power Electron.*, vol. 8, no. 3, pp. 1994–2006, Sep. 2020.

[27] D. Huang, S. Ji, and F. C. Lee, "Matrix transformer for LLC resonant converters," in *Proc. 28th Annu. IEEE Appl. Power Electron. Conf. Expo.*, 2013, pp. 2078–2083.

[28] D. Huang, S. Ji, and F. C. Lee, "LLC resonant converter with matrix transformer," in *Proc. IEEE Appl. Power Electron. Conf. Expo.*, 2014, pp. 1118–1125.

[29] B. Li, Q. Li, and F. C. Lee, "High-frequency PCB winding transformer with integrated inductors for a bi-directional resonant converter," *IEEE Trans. Power Electron.*, vol. 34, no. 7, pp. 6123–6135, Jul. 2019.

[30] M. K. Ranjram, I. Moon, and D. J. Perreault, "Variable-inverter-rectifier-transformer: A hybrid electronic and magnetic structure enabling adjustable high step-down conversion ratios," *IEEE Trans. Power Electron.*, vol. 33, no. 8, pp. 6509–6525, Aug. 2018.

[31] L. H. Dixon, Jr., "How to design a transformer with fractional turns," Unitrode/TI Magnetics Design Handbook, Texas Instruments Incorporated, Dallas, TX, USA, 2000.

[32] S. Li, E. Rong, Q. Min, and S. Lu, "A half-turn transformer with symmetry magnetic flux for high-frequency-isolated DC/DC converters," *IEEE Trans. Power Electron.*, vol. 33, no. 8, pp. 6467–6470, Aug. 2018.

[33] E. Rong, S. Li, R. Zhang, X. Du, Q. Min, and S. Lu, "A magnetic integration half-turn planar transformer for LLC resonant DC-DC converters," in *Proc. IEEE Appl. Power Electron. Conf. Expo.*, 2018, pp. 484–488.

[34] Y. Liu *et al.*, "Quarter-turn transformer design and optimization for high power density 1-MHz LLC resonant converter," *IEEE Trans. Ind. Electron.*, vol. 67, no. 2, pp. 1580–1591, Feb. 2020.

[35] W. Feng, P. Mattavelli, and F. C. Lee, "Pulsewidth locked loop (PWLL) for automatic resonant frequency tracking in LLC DC–DC transformer (LLC -DCX)," *IEEE Trans. Power Electron.*, vol. 28, no. 4, pp. 1862–1869, Apr. 2013.

[36] C. Fei, M. H. Ahmed, F. C. Lee, and Q. Li, "Two-stage 48 V-12 V/6 V-1.8 V voltage regulator module with dynamic bus voltage control for light-load efficiency improvement," *IEEE Trans. Power Electron.*, vol. 32, no. 7, pp. 5628–5636, Jul. 2017.

[37] P. L. Dowell, "Effects of eddy currents in transformer windings," *Proc. Inst. Elect. Eng.*, vol. 113, no. 8, pp. 1387–1394, Aug. 1966.

Yu-Chen Liu (Senior Member, IEEE) received the M.S. and Ph.D. degrees in electronic and computer engineering from the National Taiwan University of Science and Technology (NTUST), Taipei, Taiwan, in 2009 and 2015, respectively.

He was a Visiting Researcher with the Future Energy Electronics Center, Virginia Tech, Blacksburg, VA, USA, in 2014. From 2015 to 2016, he was a Research Assistant Professor with the Power Electronics Laboratory, Department of Electronic Engineering, NTUST. He is currently an Assistant Professor with the Department of Electrical Engineering, National Ilan University, Yilan, Taiwan.

Dr. Liu was the recipient the Young Researcher Award in 2018 from the National Science Council of Taiwan. He was a Faculty Advisor for Student Teams of the IEEE International Future Energy Challenge, receiving Awards in 2015, 2016, and 2017. He was the Chair of the IEEE Industrial Applications Society Taipei Chapter for 2017–2018.

Chen Chen (Student Member, IEEE) was born in Taipei, Taiwan, in 1991. He received the M.S. degree in electronic engineering in 2016 from the National Taiwan University of Science and Technology, Taipei, where he is currently working toward the Ph.D. degree.

From 2019 to 2020, he was a Visiting Researcher with the Center for Power Electronics Systems, Virginia Tech, Blacksburg, VA, USA. His research interests include zero-voltage-switching dc–dc converter analysis and design, wide bandgap device applications, high-frequency converters, and high-efficiency magnetic component design.

Kai-De Chen (Student Member, IEEE) was born in Tainan, Taiwan, in 1993. He received the B.S. degree in electronic engineering in 2016 from the National Taiwan University of Science and Technology, Taipei, Taiwan, where he is currently working toward the Ph.D. degree by direct pursuit.

From 2019 to 2020, he was a Visiting Researcher with the Milan M. Jovanovic Power Electronics Laboratory, Durham, NC, USA. His current research interests include resonant converters, wireless power transfer, wide bandgap device applications, and high-frequency power conversion.

Yong-Long Syu (Student Member, IEEE) was born in Tainan, Taiwan, in 1993. He received the B.S. degree in electronic engineering in 2016 from the National Taiwan University of Science and Technology, Taipei, Taiwan, where he is currently working toward the Ph.D. degree by direct pursuit.

From 2019 to 2020, he was a Visiting Researcher with the Department of Electrical Engineering and Computer Sciences, UC Berkeley, Berkeley, CA, USA. His research interests include power factor correction, resonant converters, wide bandgap device applications, and high-frequency power conversion.

De-Jia Lu was born in Taoyuan, Taiwan, in 1990. He received the M.S. degree in electronic engineering from the National Taiwan University of Science and Technology, Taipei, Taiwan, in 2019.

Since September 2019, he has been with 3Y Electronics, Inc., Irvine, CA, USA, where he is currently an Electronic Engineer. His research interests include inverters, resonant converters, and wide bandgap device applications.

Katherine A. Kim (Senior Member, IEEE) received the B.S. degree from the Franklin W. Olin College of Engineering, Needham, MA, USA, in 2007, and the M.S. and Ph.D. degrees from the University of Illinois, Urbana-Champaign, IL, USA, in 2011 and 2014, respectively, all in electrical and computer engineering.

From 2014 to 2018, she was an Assistant Professor of Electrical and Computer Engineering with the Ulsan National Institute of Science and Technology (UNIST), Ulsan, South Korea. Since 2019, she has been an Associate Professor of Electrical Engineering with National Taiwan University, Taipei, Taiwan. Her research interests include power electronics and control for solar photovoltaic applications.

Dr. Kim was a recipient of the Graduate Research Fellowship in 2011 from the U.S. National Science Foundation. She was also a recipient of the Outstanding Teaching Award from UNIST in 2015 and the Richard M. Bass Outstanding Young Power Electronics Engineer Award from the IEEE Power Electronics Society (PELS) in 2019, and received recognition as an Innovator Under 35 for the Asia Pacific Region by the MIT Technology Review in 2020. Since 2017, she has been an Associate Editor for the IEEE TRANSACTIONS ON POWER ELECTRONICS. For IEEE PELS, she was the Student Membership Chair from 2013 to 2014, PELS Member-at-Large from 2016 to 2018, and PELS Women in Engineering Chair from 2018 to 2020.

Huang-Jen Chiu (Senior Member, IEEE) received the B.E. and Ph.D. degrees from the Electronic Engineering Department at Taiwan University of Science and Technology, Taipei, Taiwan, in 1996 and 2000, respectively.

He has been with the Department of Electronic and Computer Engineering, National Taiwan University of Science and Technology (NTUST), Taipei, Taiwan, where he is a Distinguished Professor and the Director of Center for Power Electronic Technologies. He is also the Dean of Industry–Academia Collaboration with NTUST.

Dr. Chiu's work brought him several distinctive awards including the Young Researcher Award in 2004 from the Ministry of Science and Technology, Taiwan, the Outstanding Teaching Awards in 2009 and 2017, and the Excellent Research Award in 2009 and 2011 from the NTUST, the Y. Z. Hsu Scientific Paper Award in 2010, the Excellent Industry–Academia Collaboration Award in 2015 and 2017, the Outstanding Industry–Academia Collaboration Award in 2018, and Google Little Box Academic Awards. His student teams won the Grand Prize of the IEEE International Future Energy Challenge (IFEC) in 2013 and 2015, and the 2018 IEEE Empower a Billion Lives (EBL) Pacific Asia Regional Award. He is an Associate Editor for the IEEE TRANSACTIONS ON INDUSTRY APPLICATIONS. He is actively working in IEEE Taipei Section. He arranged several meetings to promote the local activity of IEEE member in Taipei Section and to increase the number of IEEE membership in Taiwan. He was the Chair of IEEE Industrial Electronics Society Taipei Chapter from 2015 to 2016, the General Co-Chair of 2017 IEEE International Future Energy Electronics Conference (IFEEC 2017-ECCE Asia), the Program Chair of 2015 IEEE IFEEC, the Topic Co-Chair of 2016 IFEC, and the Secretary of IEEE PELS/ IES Taipei Joint Chapter from 2010 to 2014. He is a fellow of the Institute of Engineering and Technology and selected as the Distinguished Lecturer of IEEE Power Electronics Society from 2017 to 2018 and from 2019 to 2020.